

Crystallographic and Electrochemical Characteristics of $\text{La}_{0.7}\text{Mg}_{0.3}\text{Ni}_{5.5-x}(\text{Al}_{0.5}\text{Mo}_{0.5})_x$ ($x = 0$ to 0.8) Hydrogen Storage Alloys

X.B. ZHANG, D.Z. SUN, W.Y. YIN, Y.J. CHAI, and M.S. ZHAO

The structure, hydrogen storage property, and electrochemical characteristics of the $\text{La}_{0.7}\text{Mg}_{0.3}\text{Ni}_{5.5-x}(\text{Al}_{0.5}\text{Mo}_{0.5})_x$ ($x = 0, 0.2, 0.4, 0.6, 0.8$) hydrogen storage alloys have been investigated systematically. It has been found by X-ray powder diffraction and Rietveld analysis that the alloys are multiphase and consist of impurity Ni phase and two main crystallographic phases, namely, the $\text{La}(\text{La}, \text{Mg})_2\text{Ni}_9$ phase and the LaNi_5 phase, and the lattice parameters and the cell volumes of both the $\text{La}(\text{La}, \text{Mg})_2\text{Ni}_9$ phase and the LaNi_5 phase increase with increasing Al and Mo content in the alloys. The P-C isotherm curves indicated that the hydrogen storage capacity of the alloy first increases and then decreases with increasing x , and the equilibrium pressure decreases with increasing x . The electrochemical measurements show that the maximum discharge capacity first increases from 298.5 ($x = 0$) to 328.3 mAh/g ($x = 0.6$) and then decreases to 304.7 mAh/g ($x = 0.8$). The high rate dischargeability (HRD) of the alloy electrodes increases lineally from 65.4 pct ($x = 0$) to 86.6 pct ($x = 0.8$) at the discharge current density of 1200 mA/g. Moreover, the exchange current density of the alloy electrodes also increases monotonously with increasing x by the linear polarization curves. The hydrogen diffusion coefficient in the alloy bulk, D , increases with increasing Al and Mo content and thus enhances the low-temperature dischargeability (LTD) of the alloy electrodes.

I. INTRODUCTION

HYDROGEN storage alloy has attracted considerable attention in view of its potential as a new energy storage material. Recently, nickel-metal hydride battery (Ni-MH), in which a hydrogen storage alloy is employed as a negative electrode material, has become a focus of interest as a candidate consumer-use battery by virtue of its several advantages: high reversible energy storage density, high resistance to overcharging and overdischarging, good charge/discharge kinetics, environmental compatibility, and interchangeability with nickel-cadmium battery.^[1-6] To date, almost all commercial Ni-MH batteries employ AB_5 -type alloys as negative electrode materials because of their good overall electrode properties.^[7] However, the electrochemical capacity of the AB_5 -type alloys is limited by the single CaCu_5 -type hexagonal structure,^[8] the energy densities of the Ni-MH batteries are not competing favorably with some other advanced secondary batteries. Therefore, new type alloys with higher energy density, faster activation, better rate dischargeability, and lower cost are urgently needed to replace the conventional rare earth-based AB_5 -type alloys.^[9]

Recently, Kadir *et al.*^[10,11,12] have reported the discovery of a new type of ternary alloys with the general formula of RMg_2Ni_9 (R: rare earth, Ca, Y) with PuNi_3 -type structure. It is found that some of the R-Mg-Ni-based ternary alloys can

absorb-desorb 1.8 to 1.87 wt pct H_2 and are thus regarded as promising candidates for reversible gaseous hydrogen storage.^[13,14] As to their electrochemical hydrogen storage, Chen *et al.*^[6] have studied the structure and electrochemical characteristics of $\text{LaCaMg}(\text{Ni}, \text{M})_9$ ($\text{M} = \text{Al}, \text{Mn}$) alloys, and almost at the same time, Kohno *et al.*^[15] have reported that the discharge capacity of $\text{La}_{0.7}\text{Mg}_{0.3}\text{Ni}_{2.8}\text{Co}_{0.5}$ alloy reached 410 mAh/g. However, the La-Mg-Ni-Co system hydrogen storage electrode alloys cannot be used as negative material of the Ni-MH secondary batteries due to their serious corrosion in KOH electrolyte,^[16] and hence, their cycling stability has to be upgraded for practical applications. In commercial AB_5 -type alloys, the presence of 10 wt pct Co has indeed improved the cycling life of Ni-MH batteries. However, it influences negatively the discharge capacity as well as initial activation and it constitutes about 40 pct of the material cost.^[17] Much effort has been devoted to search for a more cost-effective substitute element with high reliability to improve the cycling life of Ni-MH batteries. It is believed that Al is one of the best candidates for cobalt substitution.^[18] However, Al addition is detrimental to hydrogen diffusion from electrode surface to alloy bulk and thus inevitably decreases the high rate dischargeability of alloy electrode.^[19] It is reported that Mo addition can remarkably improve the kinetic property^[20] and also increase the electrochemical capacity of alloy electrode.^[21] Therefore, it can be expected that the overall electrochemical characteristics of the La-Mg-Ni-Co-type hydrogen storage alloys could be improved by substitution of Al and Mo for Ni in the alloys.

In this work, on the basis of our previous studies and the belief that the Al and Mo addition may result in some noticeable modification of the alloys,^[18-21] the structure and electrochemical characteristics of the $\text{La}_{0.7}\text{Mg}_{0.3}\text{Ni}_{5.5-x}(\text{Al}_{0.5}\text{Mo}_{0.5})_x$ ($x = 0, 0.2, 0.4, 0.6, 0.8$) hydrogen storage alloys have been investigated systematically.

X.B. ZHANG, W.Y. YIN, Y.J. CHAI, Ph.D.s, and M.S. ZHAO, Professor, are with the Key Laboratory of Rare Earth Chemistry and Physics, Changchun Institute of Applied Chemistry, Chinese Academy of Sciences, Changchun 130022, People's Republic of China. E-mail address: eboat@ciac.jl.cn D.Z. SUN, Ph.D., is with the State Key Laboratory of Electro-Analytical Chemistry, Changchun Institute of Applied Chemistry, Chinese Academy of Sciences.

Manuscript submitted October 4, 2004.

II. EXPERIMENTAL DETAILS

A. Alloy Preparation and X-Ray Diffraction Analysis

All alloy samples were prepared by arc melting carefully the constituent elements on a water-cooled copper hearth under argon atmosphere followed by annealing in vacuum for 100 hours at 770 °C. The purity of the metals, *i.e.*, La, Mg, Ni, Al, and Mo, is higher than 99.9 mass pct. The samples were all inverted and remelted 5 times to ensure good homogeneity. A slight excess of Mg over composition was needed in order to compensate for evaporative loss of Mg under preparation conditions. Several attempts (the extra Mg contents are 1, 2, 3, 4, and 5 pct, respectively) were done until the optimum preparative conditions (the extra Mg content is 3 pct) were found. The final composition was carefully checked by the inductively coupled plasma-atomic emission spectrometry (ICP-AES) method using a TJA Poems-type instrument (TJA). Thereafter, these alloy samples were mechanically crushed into fine powders of 300 mesh in mortar.

Crystallographic characteristics of the hydrogen storage alloys were investigated by X-ray diffraction on a Rigaku D/Max 2500 PC X-ray diffractometer (Rigaku, Japan) (Cu K_{α} radiation, Bragg-Brentano geometry, 2θ range 10 to 100 deg, step size 0.02 deg, backscattered rear graphite monochromator) using JADE5 software (Materials Data, Inc.).^[22] The lattice constants and cell volume were calculated by the RIETICA (IUCR Power Diffraction 22.21, 1997) program after internal theta calibration using silicon as the standard reference material.

B. Electrochemical Measurement

The well-mixed alloy powder and carbonyl nickel powder in weight ratio of 1:5 were pressed into the tablets as metal hydride electrode, which had diameter of 13 mm and thickness of 1.5 mm, and the weight of each electrode was about 0.9 g.

The electrochemical properties were then measured in a standard three-electrode cell consisting of a working electrode (metal hydride electrode), a counter-electrode (NiOOH/Ni(OH)₂ electrode), and a reference electrode (Hg/HgO electrode). The electrolyte in the cell was 6 M KOH aqueous solution. Charge and discharge tests were carried out on an automatic galvanostatic system (DC-5) (Shanghai Zhengfang Electronic Inc., P.R. China). The emphasis of these charge/discharge tests was on the electrochemical capacity and stability of the negative electrode; thus, the capacity of the positive electrode plate was designed to be much higher than that of the negative electrode. At 298 K, these experimental cells were first charged at a current of 60 mA/g for 7 hours following a rest for 30 minutes and were discharged at the same discharge current density to the cut-off voltage of -0.60 V vs Hg/HgO.

Pressure-composition isotherms (P-C-T) curves were obtained by converting the equilibrium potential of the metal hydride electrode to the equilibrium pressure of hydrogen on the basis of the Nernst equation using electrochemical data,^[23] as reported in Reference 24. The equilibrium potential curves were obtained by alternating the following two processes: (1) a pulse discharge of (25 mA/g × 0.25 h) and (2) a rest period until the potential became almost constant. The equilibrium potential change of approximately 30 mV corresponds to the equilibrium pressure change by one order of magnitude. Since the measured potentials have an error of 1 to 2 mV, the calculated pressure values are accurate to be within 10 pct.^[24]

To evaluate the high rate dischargeability (HRD) (in the range of 60 to 1200 mA/g), discharge capacities of the alloy electrode at different discharge current densities were measured. The HRD (percent) defined as $C_n \times 100 / (C_n + C_{60})$ was determined from the ratio of the discharge capacity C_n (with $n = 60, 240, 480, 720, 960,$ and 1200 mA/g, respectively) to the total discharge capacity defined as the sum of C_n and C_{60} , which was the additional capacity measured subsequently at 60 mA/g after C_n was measured.

For investigating the electrocatalytic activity of the hydrogen electrode reaction, the linear polarization curves of the electrode were plotted on a EG&G PARC's model 273 potentiostat/galvanostat station (EG&G) by scanning the electrode potential at the rate of 0.1 mV/s from -5 to 5 mV (vs open circuit potential) at 50 pct depth of discharge at 298 and 233 K. The polarization resistance R_p can be obtained from the slope of the linear polarization curves. Moreover, the exchange current density (I_0), which is a measure of the catalytic activity of electrode, was calculated from the slopes of polarization curves by the following equation:^[18]

$$I_0 = \frac{RT}{FR_p}$$

where R is the gas constant, T is the absolute temperature, F is the Faraday constant, and R_p is the polarization resistance. The potentiostatic discharge technique was used to evaluate the coefficient of diffusion within the bulk of the alloy electrode. After being fully charged followed by a 30-minute open-circuit lay aside, the test electrodes were discharged with a +500 mV potential step for 500 seconds on a EG&G PARC's model 273 potentiostat/galvanostat station (EG&G), using the M352 CorrWare electrochemical/corrosion software.

III. RESULTS AND DISCUSSION

A. Alloy Composition and Structure Characteristic

It is well known that the low melting Mg metal will be inevitably lost during the sample preparation by arc melting. Many ways have been tried to overcome this problem, such as using Mg-Ni master alloy as an Mg additive, decreasing the melting current, adding a slight excess of Mg over sample composition, and so on. Among all these methods, the third one is found to be the most effective way to compensate evaporative loss of Mg. In this article, the lost weight during sample preparation is almost the same as excess Mg added. The results of ICP-AES analysis for all compounds are given in Table I. It can be seen that the final composition of all the alloys is identical with the original composition.

The crystal structures of $\text{La}_{0.7}\text{Mg}_{0.3}\text{Ni}_{5.5-x}(\text{Al}_{0.5}\text{Mo}_{0.5})_x$ ($x = 0$ to 0.8) alloy have been identified by means of X-ray powder diffraction. Figure 1 shows the Rietveld refinement pattern of the XRD profiles for the $\text{La}_{0.7}\text{Mg}_{0.3}\text{Ni}_{5.3}(\text{Al}_{0.5}\text{Mo}_{0.5})_{0.2}$ hydrogen storage alloy as a representative example of $\text{La}_{0.7}\text{Mg}_{0.3}\text{Ni}_{5.5-x}(\text{Al}_{0.5}\text{Mo}_{0.5})_x$ ($x = 0$ to 0.8) hydrogen storage alloys. The result shows that, besides an impurity Ni phase, the $\text{La}_{0.7}\text{Mg}_{0.3}\text{Ni}_{5.3}(\text{Al}_{0.5}\text{Mo}_{0.5})_{0.2}$ alloy consists of two phases: a La_2MgNi_9 phase with a PuNi_3 -type rhombohedral structure and a LaNi_5 phase with a CaCu_5 -type hexagonal structure. The final Rietveld structure parameters of the alloy are tabulated in Table II. The

Table I. Composition of the $\text{La}_{0.7}\text{Mg}_{0.3}\text{Ni}_{5.5-x}(\text{Al}_{0.5}\text{Mo}_{0.5})_x$ ($x = 0$ to 0.8) Alloys

Samples	La (mg/g)	Mg (mg/g)	Ni (mg/g)	Al (mg/g)	Mo (mg/g)	La: Mg: Ni: Al: Mo*
$x = 0$	227.52	17.06	755.42	0.00	0.00	1.64:0.70:12.87:0:0
$x = 0.2$	227.23	17.04	727.01	6.30	22.42	1.64:0.70:12.39:0.23:0.23
$x = 0.4$	226.93	17.02	698.67	12.59	44.78	1.63:0.70:11.90:0.47:0.47
$x = 0.6$	226.64	17.00	670.41	18.87	67.09	1.63:0.70:11.42:0.70:0.70
$x = 0.8$	226.35	16.98	642.22	25.12	89.33	1.63:0.70:10.94:0.93:0.93

*Atomic ratio.

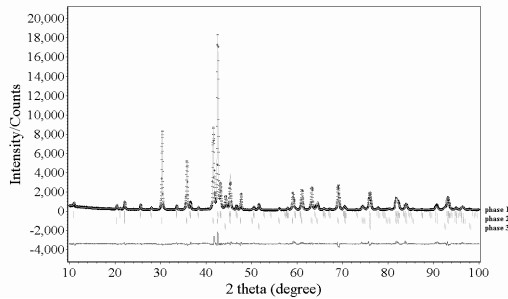


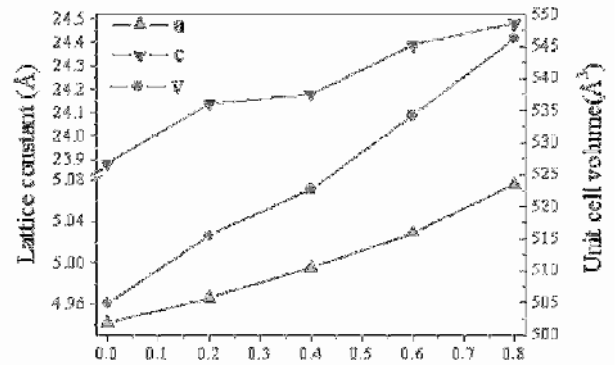
Fig. 1—Rietveld refinement pattern of the XRD profiles for the $\text{La}_{0.7}\text{Mg}_{0.3}\text{Ni}_{5.3}(\text{Al}_{0.5}\text{Mo}_{0.5})_{0.2}$ hydrogen storage alloy (phase 1: $\text{La}(\text{La}, \text{Mg})_2\text{Ni}_9$; phase 2: LaNi_5 ; and phase 3: Ni).

Table II. Crystallographic Parameters for La_2MgNi_9 by Using X-Ray Diffraction $\text{Cu } K_{\alpha 1}$ ($\lambda = 1.5405981 \text{ \AA}$) at 298 K in a Space Group $R\bar{3}m$ and $Z = 3^*$

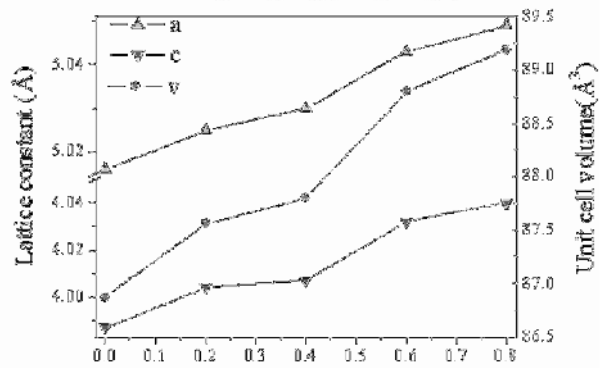
Atom	Site	Metal Atom Position			Occupancy
		x	y	z	
La1	3a	0	0	0	1
La2	6c	0	0	0.1438(3)	0.472
Mg1	6c	0	0	0.1438(3)	0.528
Ni1	6c	0	0	0.3299(2)	1
Ni2	3b	0	0	0.5	1
Ni3	18h	0.4984(1)	0.5017(1)	0.0849(4)	1

*Structure was refined by using the Rietveld refinement program Rietica. The pattern factor $R_p = 6.6$, the weighted pattern factor $R_{wp} = 8.8$, and the goodness of fit $S = 2.3$.

crystallographic results reveal that La atoms in La_2MgNi_9 are located not only at the 3a site (the Pu1 atom position of the PuNi_3 structure), but also at the 6c sites (the Pu2 atom position of the PuNi_3 structure), while Mg atoms in the alloy exhibit a strong preference for the 6c site, which implies that Mg atoms can occupy the 6c sites as well as La atoms, indicating that the alloy is a ordered compound with the same structure as the previously reported RMg_2Ni_9 ($R = \text{La}, \text{Ca}, \text{Y}$) alloys. So the final structure of La_2MgNi_9 phase can be designated as $\text{La}(\text{La}, \text{Mg})_2\text{Ni}_9$. Figure 2 shows the lattice parameters and unit cell volume of the $\text{La}_{0.7}\text{Mg}_{0.3}\text{Ni}_{5.5-x}(\text{Al}_{0.5}\text{Mo}_{0.5})_x$ alloys as a function of x . It can be seen that a and c parameters of both the $\text{La}(\text{La}, \text{Mg})_2\text{Ni}_9$ phase and the LaNi_5 phase in the alloys all increase linearly with the increase of x , which is mainly ascribed to the fact that the atomic radius of Al (1.432 Å) and Mo (1.363 Å) is larger than that of Ni (1.246 Å). Figure 3 shows the abundances of the $\text{La}(\text{La}, \text{Mg})_2\text{Ni}_9$ phase and the LaNi_5 phase as a function of x in the $\text{La}_{0.7}\text{Mg}_{0.3}\text{Ni}_{5.5-x}(\text{Al}_{0.5}\text{Mo}_{0.5})_x$ alloys. As can be seen in Figure 3, the $\text{La}(\text{La}, \text{Mg})_2\text{Ni}_9$ phase abundance



(a)



(b)

Fig. 2—Variations of the cell parameters and volumes as the function of x in $\text{La}_{0.7}\text{Mg}_{0.3}\text{Ni}_{5.5-x}(\text{Al}_{0.5}\text{Mo}_{0.5})_x$ alloys ($x = 0$ to 0.8): (a) $\text{La}(\text{La}, \text{Mg})_2\text{Ni}_9$ phase and (b) LaNi_5 phase.

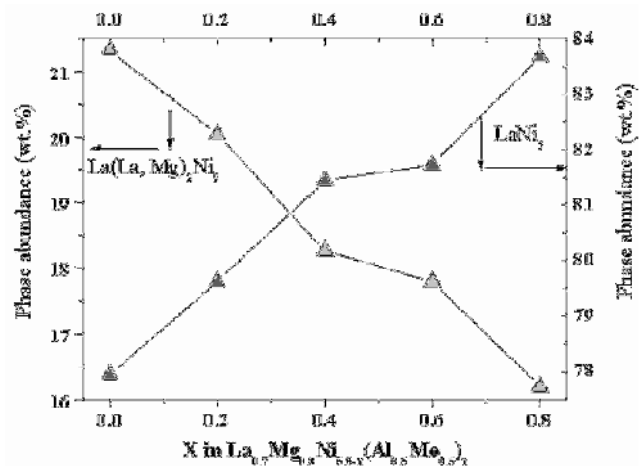


Fig. 3—Phase abundance of the $\text{La}(\text{La}, \text{Mg})_2\text{Ni}_9$ phase and the LaNi_5 phase existing in the $\text{La}_{0.7}\text{Mg}_{0.3}\text{Ni}_{5.5-x}(\text{Al}_{0.5}\text{Mo}_{0.5})_x$ ($x = 0$ to 0.8) alloys.

decreases from 21.32 to 16.20 pct with increasing x ; however, the LaNi_5 phase abundance increases from 77.95 to 83.66 pct. These results may influence the hydrogen storage performances and electrochemical characteristics of the alloys studied.

B. P-C Isotherms

The electrochemical pressure-composition isotherms method is very useful for examining the charging and discharging levels of hydrogen in an anode, although the calculated pressures pertain to a quasi-equilibrium state.^[18] Figure 4 shows the electrochemical P-C isotherms for $\text{La}_{0.7}\text{Mg}_{0.3}\text{Ni}_{5.5-x}(\text{Al}_{0.5}\text{Mo}_{0.5})_x$ ($x = 0$ to 0.8) alloy electrodes at 298 K. It can be seen that the desorption pressure reduces continually as the Al and Mo additions increase. This means that the stability of the hydrides of alloys increases with the increasing Al and Mo content because of the larger unit cell volume of the alloy with increasing Al and Mo additions. The phenomenon observed here is consistent with those reported previously for AB_3 alloys^[14] and most AB_5 alloys.^[25] Moreover, it can be seen that there is only one plateau in each P-C-T curve, as shown in Figure 4. Since the unit cell of the AB_3 compounds contains one-third AB_5 structure and two-thirds AB_2 structure,^[6] it is possible that the plateau pressure of the $\text{La}(\text{La}, \text{Mg})_2\text{Ni}_9$ phase is similar to that of the LaNi_5 phase.

When x increases from 0 to 0.6, the hydrogen storage capacity of the $\text{La}_{0.7}\text{Mg}_{0.3}\text{Ni}_{5.5-x}(\text{Al}_{0.5}\text{Mo}_{0.5})_x$ ($x = 0, 0.2, 0.4, 0.6, 0.8$) alloy first increases from 0.732 to 0.808 wt pct, which is mainly attributed to the decrease in plateau pressure, which enhances the intrinsic hydrogen storage capacity of alloys. However, as x reaches 0.8, the hydrogen storage capacity decreases to 0.751 wt pct, which can be attributed to the change in the relative amounts of $\text{La}(\text{La}, \text{Mg})_2\text{Ni}_9$ phase and LaNi_5 phase owing to Al and Mo substitution. It is known that the LaNi_5 phase works not only as a hydrogen reservoir but also as a catalyst to activate the $\text{La}(\text{La}, \text{Mg})_2\text{Ni}_9$ phase to reversibly absorb/desorb hydrogen in the alkaline electrolyte.^[26] Therefore, it is believed that there is an optimum relative content of the $\text{La}(\text{La}, \text{Mg})_2\text{Ni}_9$ phase and the LaNi_5 phase for improving the overall properties of the

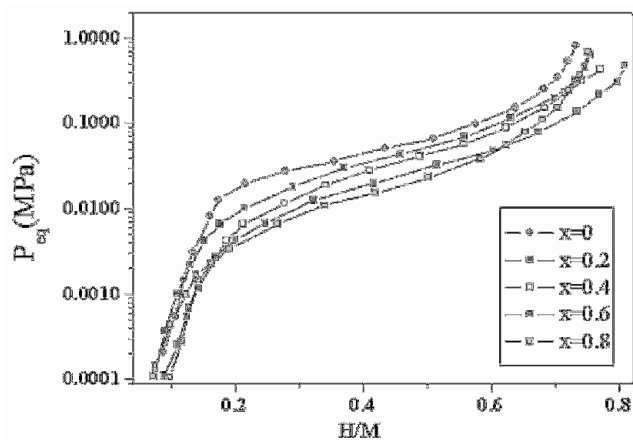


Fig. 4—Electrochemical desorption P-C-T curves for $\text{La}_{0.7}\text{Mg}_{0.3}\text{Ni}_{5.5-x}(\text{Al}_{0.5}\text{Mo}_{0.5})_x$ ($x = 0$ to 0.8) alloy electrodes at 298 K.

La-Mg-Ni-Al-Mo -type hydrogen storage alloys. The recommended amount of Al and Mo addition is 0.6 from our work.

C. Discharge Performance and Cyclic Stability

The cycle numbers needed to activate the electrodes and maximum discharge capacity of the $\text{La}_{0.7}\text{Mg}_{0.3}\text{Ni}_{5.5-x}(\text{Al}_{0.5}\text{Mo}_{0.5})_x$ ($x = 0$ to 0.8) alloy electrodes are listed in Table III. It can be seen that all of these alloys can be easily activated to reach the maximum capacity within four cycles. For the alloys with composition range of $x = 0$ to 0.8, the maximum discharge capacity C_{max} improves significantly with the increase in x and reaches a maximum at $x = 0.6$, and then decreases as x increases further. The variation of maximum discharge capacity of the alloys is consistent with the variation of the H/M with the Al and Mo content in the alloys. The $\text{La}_{0.7}\text{Mg}_{0.3}\text{Ni}_{4.9}(\text{Al}_{0.5}\text{Mo}_{0.5})_{0.6}$ alloy shows a maximum discharge capacity of 328.3 mAh/g, which is noticeably higher than that of the commercial AB_5 -type alloys.

Figure 5 shows the discharge curves (fifth cycle) of the $\text{La}_{0.7}\text{Mg}_{0.3}\text{Ni}_{5.5-x}(\text{Al}_{0.5}\text{Mo}_{0.5})_x$ ($x = 0$ to 0.8) alloy electrodes at 60 mA/g and 298 K. Obviously, each curve has a wide discharge potential plateau based on the oxidation of desorbed hydrogen from the hydride. Besides, the discharge plateau shifts toward a more positive potential as Al and Mo addition

Table III. Summary of the Electrode Performance of $\text{La}_{0.7}\text{Mg}_{0.3}\text{Ni}_{5.5-x}(\text{Al}_{0.5}\text{Mo}_{0.5})_x$ ($x = 0$ to 0.8) Alloy Electrodes

Samples	H/M	C_{max} (mAh/g)	N_a^*	HRD ₁₂₀₀ ** (Pct)	S_{70} (Pct)
$x = 0.0$	0.732	298.5	4	65.4	52.1
$x = 0.2$	0.755	307.4	3	68.5	58.9
$x = 0.4$	0.769	312.9	3	74.5	63.9
$x = 0.6$	0.808	328.3	2	82.8	68.1
$x = 0.8$	0.751	304.7	2	86.6	72.7

*The cycle numbers needed to activate the electrodes.

**The high rate dischargeability at the discharge current density of 1200 mA/g.

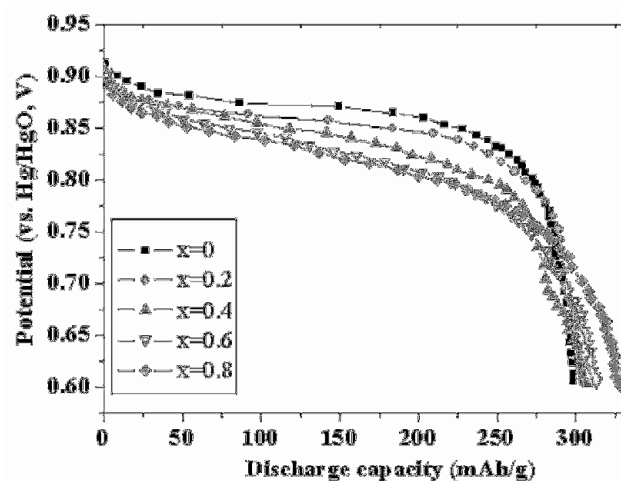


Fig. 5—Discharge curves of $\text{La}_{0.7}\text{Mg}_{0.3}\text{Ni}_{5.5-x}(\text{Al}_{0.5}\text{Mo}_{0.5})_x$ ($x = 0$ to 0.8) alloy electrodes at the discharge current density of 60 mA/g and 298 K.

increases in the alloys. As shown in Figure 5, the middle-discharge (potential at 50 pct depth of discharge) potential decreases from -0.8711 to -0.8182 V when x increases from 0 to 0.8, in agreement with the reduction of desorption plateau pressure when x increases from 0 to 0.8 in the alloys.

The cycling capacity retention rate, expressed as S_{70} (pct) = $C_{70}/C_{\max} \times 100$ (where C_{\max} is the maximum discharge capacity, and C_{70} is the discharge capacity at the seventieth cycle) after 70 cycles at 60 mA/g, is also listed in Table III. As seen in Table III, the capacity retention rate (S_{70}) increases noticeably from 52.1 to 72.7 pct with x increasing from 0 to 0.8, indicating that the cyclic stability of the La-Mg-Ni-Al-Mo system alloys is improved markedly with the increase of Al and Mo content in the alloys. It is known that the capacity degradation of La-Mg-Ni-type alloy electrode results primarily from two factors, the corrosion of Mg and La elements and the pulverization of the alloy particles.^[25] The Al substitution results in the formation of protective oxide (hydroxide) of Al on the alloy surface and a subsequent strong protection to the alloy from further corrosion of La and Mg. Moreover, the pulverization of the alloy particles can be improved effectively by Mo substitution for Ni. In conclusion, the combined effect of Al and Mo addition results in the notable improvement of the alloy electrodes. Further investigations in this aspect are occurring in our research group.

D. HRD and Low-Temperature Dischargeability

As an important kinetics property of the hydride electrode in battery, it is very important to hold back the decrease of the discharge capacity even at the high charge/discharge current density. Figure 6 shows the relationship between the HRD and the discharge current density of the $\text{La}_{0.7}\text{Mg}_{0.3}\text{Ni}_{5.5-x}(\text{Al}_{0.5}\text{Mo}_{0.5})_x$ ($x = 0$ to 0.8) alloy electrodes. The HRD of the alloy electrodes for the discharge current density of 1200 mA/g are also listed in Table III. It can be seen that as the x increases, the HRD of the alloy electrodes increases from 65.4 pct ($x = 0$) to 86.6 pct ($x = 0.8$). It is well known that the HRD of metal hydride electrode is influenced mainly by the electrochemical reaction kinetics on the alloy powder

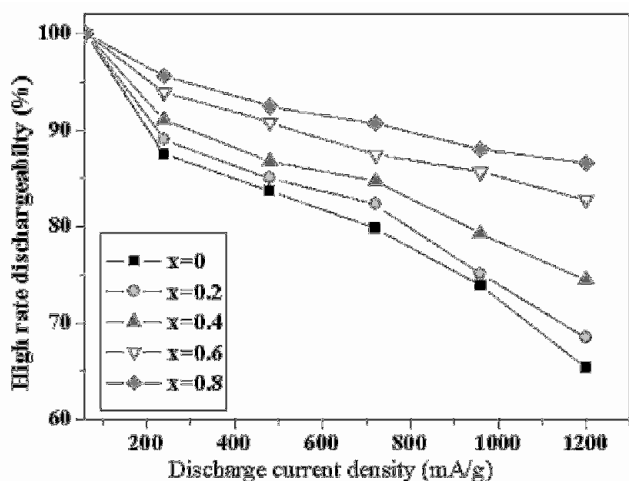


Fig. 6—HRD of the $\text{La}_{0.7}\text{Mg}_{0.3}\text{Ni}_{5.5-x}(\text{Al}_{0.5}\text{Mo}_{0.5})_x$ ($x = 0$ to 0.8) alloy electrodes at 298 K.

surface and the diffusion rate of hydrogen in the bulk of the alloy.^[27] To examine the effect of the partial substitution of Al and Mo for Ni on the discharge kinetics, linear polarization was performed on these alloy electrodes. Based on the measured linear polarization curves, values of exchange current density I_0 and polarization resistance R_p were evaluated for $\text{La}_{0.7}\text{Mg}_{0.3}\text{Ni}_{5.5-x}(\text{Al}_{0.5}\text{Mo}_{0.5})_x$ ($x = 0$ to 0.8) alloy electrodes and are summarized in Table IV. Figure 7 shows HRD and polarization resistance, R_p , as a function of the exchange current density, I_0 , for the hydrogen evolution reaction at the $\text{La}_{0.7}\text{Mg}_{0.3}\text{Ni}_{5.5-x}(\text{Al}_{0.5}\text{Mo}_{0.5})_x$ ($x = 0$ to 0.8) alloy electrodes. The HRD is a linear function of I_0 and the hydrogen diffusion coefficient (D) remains nearly unchanged (14.1 to 14.9×10^{-10} cm²/s). Iwakura *et al.*^[28] have pointed out that if the electrochemical reaction on the surface is a rate-determining factor, a linear dependence of the HRD on the exchange current density should be observed. In contrast, if the diffusion of hydrogen in the bulk is a rate-determining factor, the HRD should be constant, irrespective of exchange density. Therefore, in the present study, the HRD is essentially controlled by the charge-transfer reaction of hydrogen on the surface at a discharge current density of 1200 mA/g. Alternatively, Figure 7 demonstrates that the polarization resistance R_p decreases under increasing exchange current density; while, conversely, the ability of discharge increases, all of which implies that the R_p value is closely related to the HRD.

Table IV. Electrochemical Kinetic Parameters of $\text{La}_{0.7}\text{Mg}_{0.3}\text{Ni}_{5.5-x}(\text{Al}_{0.5}\text{Mo}_{0.5})_x$ ($x = 0$ to 0.8) Alloy Electrodes

Samples	Exchange Current Density, I_0 (mA/g)		Hydrogen Diffusion Coefficient, D ($\times 10^{-10}$ cm ² /s)	
	298 K	233 K	298 K	233 K
$x = 0.0$	270.99	84.32	14.1	1.9
$x = 0.2$	274.33	84.65	14.1	3.5
$x = 0.4$	294	84.93	14.3	4.2
$x = 0.6$	312.83	85.07	14.8	5.5
$x = 0.8$	319	85.27	14.9	6.3

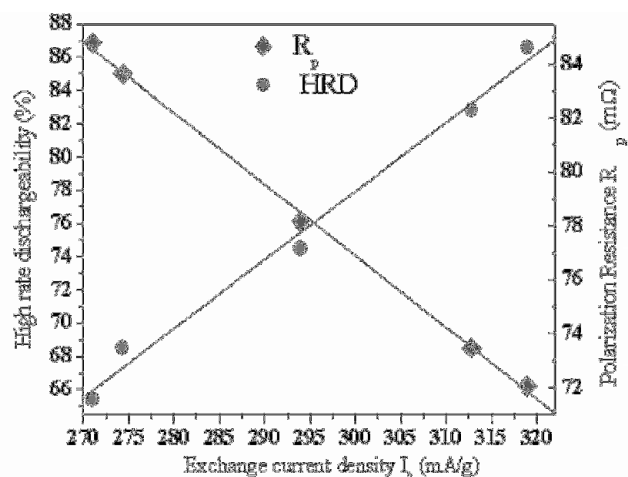


Fig. 7—HRD and polarization resistance as a function of exchange current density for hydrogen evolution reaction at $\text{La}_{0.7}\text{Mg}_{0.3}\text{Ni}_{5.5-x}(\text{Al}_{0.5}\text{Mo}_{0.5})_x$ ($x = 0$ to 0.8) alloy electrodes.

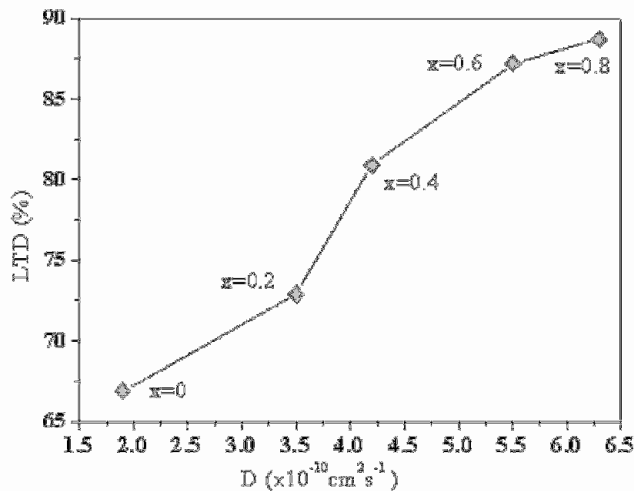


Fig. 8—LTD as a function of hydrogen diffusion coefficient (D) of the $\text{La}_{0.7}\text{Mg}_{0.3}\text{Ni}_{5.5-x}(\text{Al}_{0.5}\text{Mo}_{0.5})_x$ ($x = 0$ to 0.8) alloy electrodes at 233 K.

It has been reported that the discharge capacity of the negative electrode in nickel-metal hydride decreases drastically with decreasing temperature.^[29] Sakai *et al.*^[2] pointed out that the dischargeability of the negative electrodes at relatively low temperature depended on the hydrogen diffusion or charge-transfer process occurring at the metal electrolyte interface. The hydrogen diffusion coefficient (D) of hydrogen in the alloy bulk is evaluated using the method described by Iwakura *et al.*^[30] The low-temperature dischargeability (LTD) is expressed as $\text{LTD}_{233}(\text{pct}) = C_{233}/C_{298} \times 100$ (where C_{233} and C_{298} are the discharge capacity at 233 and 298 K, respectively). The hydrogen diffusion coefficient (D) and the exchange current density (I_0) of the alloy electrodes at 233 K are also listed in Table IV. It can be found that both the I_0 and the D are smaller than those at 298 K, respectively, and the I_0 remains nearly unchanged (84.32 to 85.27 mA/g) but the D increases remarkably with increasing x , which implies that the hydrogen diffusion in alloy probably becomes the rate-determining factor for LTD at 233 K. Figure 8 shows the LTD as a function of D in the alloy electrodes. It can be easily found that the D increases with the increases of x , which can be attributed to the cell volume expansion with increasing x . The larger D accordingly increases the LTD of the alloy electrodes.

IV. CONCLUSIONS

The effect of Al and Mo substitution for Ni on the structure, hydrogen storage property, and electrochemical characteristics of the $\text{La}_{0.7}\text{Mg}_{0.3}\text{Ni}_{5.5-x}(\text{Al}_{0.5}\text{Mo}_{0.5})_x$ ($x = 0$ to 0.8) hydrogen storage alloys have been studied systematically. X-ray diffraction Rietveld analysis shows that all the alloys consist of a $\text{La}(\text{La}, \text{Mg})_2\text{Ni}_9$ phase and the LaNi_5 phase. The pressure-composition isotherm curves indicate that the hydrogen storage capacity first increases and then decreases with increasing x , and the equilibrium pressure decreases with increasing x . Electrochemical measurements show that the maximum discharge capacity increases from 298.5 ($x = 0$) to 328.3 mAh/g ($x = 0.6$) and then decreases to 304.7 mAh/g ($x = 0.8$). For the discharge current density of 1200 mA/g,

the HRD of the alloy electrodes increases linearly from 65.4 pct ($x = 0$) to 86.6 pct ($x = 0.8$). Moreover, according to the linear polarization curves, the exchange current density of the alloy electrodes also increases monotonously with increasing x . Moreover, the LTD of the alloy electrodes increases monotonically with increasing x in the alloys.

ACKNOWLEDGMENTS

This work was financially supported by the National Natural Science Foundation of China (Grant No. 20171042).

REFERENCES

- J.J.G. Willems and K.H.J. Buschow: *J. Less-Common Met.*, 1987, vol. 129, pp. 13-30.
- T. Sakai, H. Miyamura, N. Kuriyama, A. Kato, K. Oguro, and H. Ishikawa: *J. Electrochem. Soc.*, 1990, vol. 137, pp. 795-99.
- T. Kohno, H. Yoshida, F. Kawashima, T. Inaba, I. Sakai, M. Yamamoto, and M. Kanda: *J. Alloys Compounds*, 2000, vol. 311, pp. L5-L17.
- J.J.G. Willems: *Philips J. Res.*, 1984, vol. 39 (Suppl. 1), pp. 1-94.
- H.G. Pan, Y.F. Zhu, M.X. Gao, and Q.D. Wang: *J. Electrochem. Soc.*, 2002, vol. 149, pp. A829-A833.
- J. Chen, N. Kuriyama, H.T. Takeshita, H. Tanaka, T. Sakai, and M. Haruta: *Electrochem. Solid-State Lett.*, 2000, vol. 3, pp. 249-52.
- T. Sakai, I. Uehara, and H. Iwakura: *J. Alloys Compounds*, 1999, vols. 293-295, pp. 762-69.
- J.J. Reilly, G.D. Adzic, J.R. Johnson, T. Vogt, S. Mukerjee, and J. McBreen: *J. Alloys Compounds*, 1999, vols. 293-295, pp. 569-82.
- Y.F. Liu, H.G. Pan, Y.F. Zhu, R. Li, and Y.Q. Lei: *Mater. Sci. Eng. A*, 2004, vol. A372, pp. 163-72.
- K. Kadir, T. Sakai, and I. Uahara: *J. Alloys Compounds*, 1997, vol. 257, pp. 115-21.
- K. Kadir, N. Nuriyama, T. Sakai, I. Uehara, and L. Eriksson: *J. Alloys Compounds*, 1999, vol. 284, pp. 145-54.
- K. Kadir, T. Sakai, and I. Uahara: *J. Alloys Compounds*, 1999, vol. 287, pp. 264-70.
- K. Kadir, T. Sakai, and I. Uahara: *J. Alloys Compounds*, 2000, vol. 302, pp. 112-17.
- J. Chen, H.T. Takeshita, H. Tanaka, N. Kuriyama, and T. Sakai: *J. Alloys Compounds*, 2000, vol. 302, pp. 304-13.
- T. Kohno, H. Yoshida, F. Kawashima, T. Inaba, I. Sakai, M. Yamamoto, and M. Kanda: *J. Alloys Compounds*, 2000, vol. 311, pp. L5-L17.
- B. Liao, Y.Q. Lei, L.X. Chen, G.L. Lu, H.G. Pan, and Q.D. Wang: *J. Power Sources*, 2004, vol. 129, pp. 358-67.
- P.H. Notton and P. Hokkeling: *J. Electrochem. Soc.*, 1991, vol. 138, pp. 1877-85.
- T. Sakai, H. Miyamura, N. Kuriyama, A. Kato, K. Oguro, and H. Ishikawa: *J. Less-Common Met.*, 1990, vol. 159, pp. 127-39.
- T. Sakai, H. Miyamura, N. Kuriyama, A. Kato, K. Oguro, and H. Ishikawa: *J. Electrochem. Soc.*, 1990, vol. 137, pp. 795-99.
- C. Iwakura, H. Senoh, K. Morimoto, Y. Hara, and H. Inoue: *Electrochem.*, 2002, vol. 70, pp. 2-7.
- M.T. Yeh, V.M. Beibutian, and S.E. Hsu: *J. Alloys Compounds*, 1999, vols. 293-295, pp. 721-23.
- Materials Data JADE Release 5, XRD Pattern Processing, Materials Data Inc. (MDI), 1997.
- J. Balej: *Int. J. Hydrogen Energy*, 1985, vol. 10, pp. 365-69.
- C. Iwakura, T. Asaoka, H. Yoneyama, T. Sakai, K. Oguro, and H. Ishikawa: *Nippon Kagaku Kaishi*, 1988, vol. 8, pp. 1482-88.
- J.J. Reilly: in *Handbook of Battery Materials*, Metal Hydrides Electrodes, ed., Wiley, New York, NY, 2000, pp. 327-31.
- H.G. Pan, Y.F. Liu, M.X. Gao, Y.Q. Lei, and Q.D. Wang: *J. Electrochem. Soc.*, 2003, vol. 150, pp. A565-A570.
- T. Sakai, H. Miyamura, N. Kuriyama, A. Kato, K. Oguro, and H. Ishikawa: *J. Less-Common Met.*, 1990, vol. 159, pp. 127-39.
- C. Iwakura, T. Oura, H. Inoue, and M. Matsuoka: *Electrochim. Acta*, 1996, vol. 41, pp. 117-21.
- H. Senoh, Y. Hara, H. Inoue, and C. Iwakura: *Electrochim. Acta*, 2001, vol. 46, pp. 967-71.
- C. Iwakura, H. Senoh, K. Morimoto, Y. Hara, and H. Inoue: *Electrochemistry*, 2002, vol. 70, pp. 2-7.